Cellular and Molecular Neurobiology (2025) 45:48
https://doi.org/10.1007/s10571-025-01571-z

ORIGINAL RESEARCH

Prognostic Role of Cuproptosis-Related Gene after Intracerebral Hemorrhage in Mice

Xi Shen[1] · Jiandong Zhu[1] · Yuhang Gu[1] · Jinxin Lu[1] · Weiwei Zhai[1] · Liang Sun[1] · Jiang Wu[1] · Zhengquan Yu[1]

Received: 2 October 2024 / Accepted: 12 May 2025

Abstract

Intracerebral hemorrhage (ICH) is a highly fatal form of stroke for which there are limited effective treatments. Cuproptosis, a newly discovered type of programmed cell death, has not yet been investigated in relation to ICH. Thus, the main goal of our study was to investigate the involvement of cuproptosis-related genes (CRGs) in predicting the early outcomes of ICH. We used datasets GSE228222 and GSE200575 from the Gene Expression Omnibus (GEO) database to identify and analyze differentially expressed genes (DEGs) between ICH samples and control samples from mice. From this analysis, seven cuproptosis-related DEGs (CuDEGs) were identified: pyruvate dehydrogenase E1 component subunit alpha (Pdha1), glutaminase (Gls), dihydrolipoamide dehydrogenase (Dld), pyruvate dehydrogenase E1 component subunit beta (Pdhb), dihydrolipoamide S-acetyltransferase (Dlat), metal regulatory transcription factor 1(Mtf1), and solute carrier family 31 member 1 (Slc31a1). Pathway enrichment analysis connected these genes to metabolic pathways, while immune cell infiltration analysis revealed increased macrophages and naive CD8 T cells alongside reduced NK resting cells and CD4 T cells in ICH samples. Verification through qRT-PCR and immunohistochemistry demonstrated a lower expression of CuDEGs in ICH samples. Of particular note, Gls, a gene significantly linked to both cuproptosis and immune regulation, exhibited reduced expression, possibly reflecting a protective response to limit glutamate production and mitigate neuronal damage. In summary, Gls emerges as a promising target for improving ICH outcomes by regulating cuproptosis and immune activity. This research provides novel insights into the molecular processes involved in ICH and suggests potential therapeutic approaches.

Keywords Cuproptosis · Intracerebral hemorrhage · Gls · Immune infiltration

Introduction

Intracerebral hemorrhage (ICH) constitutes about 25% of all stroke cases, with a high mortality rate, and many survivors suffer from varying degrees of disability (Li et al. 2021; Cordonnier et al. 2018). The initial or primary injury in ICH refers to the mechanical deformation and destruction of brain tissue caused by the expanding hematoma (Xi et al. 2006). Following this, secondary injury continues to cause brain damage and neuronal death, driven by perihemorrhagic inflammation, hematotoxic product breakdown, and the development of perihematoma edema (Keep et al. 2012; Lim-Hing et al. 2017). Neuroinflammation is a critical factor contributing to secondary brain injury after ICH. Animal studies have demonstrated that the endogenous hematoma clearance system becomes active post-ICH, primarily through the phagocytosis of inflammatory cells (Han et al. 2023). Additionally, monocyte-derived macrophages and neutrophils from the peripheral blood infiltrate the hematoma and surrounding brain tissue (Wilkinson et al. 2018). Neuronal necrosis, driven by a variety of pro-inflammatory mediators, is a major cause of functional impairment after ICH, and it intensifies the conditions leading to neuronal death (Zille et al. 2017). As such, targeting the neuroinflammatory response and mitigating inflammatory neuronal necrosis represent promising strategies for improving functional outcomes after ICH.

Xi Shen and Jiandong Zhu have contributed equally to this work.

✉ Jiandong Zhu
chanton.zhu@neurosci.com.cn

✉ Jiang Wu
szjiangwu@163.com

✉ Zhengquan Yu
zhengquan.yu@neurosci.com.cn

[1] Department of Neurosurgery, The First Affiliated Hospital of Soochow University, Suzhou, China

Published online: 22 May 2025

Copper, a vital micronutrient in the human body, serves as a crucial enzymatic cofactor involved in essential biological processes, including mitochondrial respiration, antioxidant defense, and the synthesis of biomolecules. The concentration of copper is tightly regulated within a narrow range, as abnormal accumulation of copper ions can lead to severe cytotoxicity (Zille et al. 2017). Cuproptosis, a newly identified type of programmed cell death, occurs when Copper ions directly interact with fatty acylated components of the tricarboxylic acid (TCA) cycle during mitochondrial respiration. This interaction leads to the accumulation of fatty acylated proteins and inhibits the function of iron-sulfur cluster proteins, which ultimately triggers cell death (Tsvetkov et al. 2022; Tang et al. 2022). However, the precise mechanisms of cuproptosis are not yet fully understood.

Several types of cell death, including ferroptosis, may occur after ICH, collectively contributing to neuronal death. Ferroptosis, specifically, is distinguished by an increase in reactive oxygen species (ROS) levels within cells (Lin et al. 2023). Previous research has demonstrated that cuproptosis plays a role in the pathological regulation of various diseases, such as osteoarthritis, rheumatoid arthritis (Han et al. 2024), and diabetic nephropathy (Xu et al. 2023), all of which are also associated with increased intracellular ROS levels. This suggests a potential link between cuproptosis and ferroptosis. Given that both processes involve metal ion-induced programmed cell death, it is proposed that cuproptosis could play a crucial role in the pathophysiology of ICH, although the precise mechanisms underlying this process have yet to be fully understood.

To investigate potential prognostic mechanisms, we utilized the Gene Expression Omnibus (GEO) database to analyze differentially expressed genes (DEGs) in control and ICH samples from mice. We then identified the DEGs and cross-referenced them with cuproptosis-related genes (CRGs) to discover differentially expressed cuproptosis-related DEGs (CuDEGs). Pathway enrichment analysis was conducted to explore the potential biological pathways involved. Additionally, we validated our findings using human data from the GSE24265 dataset. Finally, we examined the connection between cuproptosis and immune cell infiltration, offering a novel perspective for understanding the molecular mechanisms underlying ICH prognosis.

Materials and Methods

Data Collection and Processing

We retrieved the GSE228222, GSE220575, and GSE24265 datasets from the Gene Expression Omnibus database (GEO, https://www.ncbi.nlm.nih.gov/geo/). The GSE228222 and GSE220575 datasets, consisting of six ICH samples and six control samples, were combined to form a training set. Batch effects were calculated using the"sva"package (version 3.48.0), and the datasets were normalized by batch correction with the Combat function (version 0.0.4). Differential gene expression analysis was performed using the R package"limma"(version 3.56.2), with a selection threshold for DEGs set at adj. $P < 0.05$ and $|\log_2 FC| > 1.5$. CRGswere sourced from the existing literature (Tsvetkov et al. 2022; Liu et al. 2022).

Functional Enrichment Analysis

We conducted functional enrichment analysis of the DEGs using WebGestalt (http://webgestalt.org/). Gene Set Enrichment Analysis (GSEA) was employed to analyze genome-wide expression profiling microarray data, comparing the identified genes to predefined gene sets (Debrabant et al. 2017). The Kyoto Encyclopedia of Genes and Genomes (KEGG) database was used to explore the complex interactions and functional dynamics of biological systems at the gene level, offering insights into the pathways connecting various biological components (Kanehisa et al. 2000). Additionally, Gene Ontology (GO) analysis was performed to categorize the functional roles of genes and proteins, covering three main aspects: biological process (BP), cellular component (CC), and molecular function (MF) (The Gene Ontology Resource 2019). Both GO and KEGG enrichment analyses were conducted using the"ClusterProfiler"package (version 4.8.2) in R software (Yu et al. 2012). By utilizing these different enrichment tools, which operate on distinct algorithms, we were able to cross-validate the findings from each analysis method.

Evaluation of Immune Cell Infiltration

In this study, we initially evaluated the proportions of 22 different immune cell types in control and ICH samples from the merged database using the CIBERSORT algorithm. To further extend our analysis beyond GSEA, we employed single-sample gene set enrichment analysis (ssGSEA) to generate 23 immune-related gene sets. The immunological profile of all samples was then examined using the"GSVA"R package (version 1.48.3) (Hänzelmann et al. 2013). This approach provided a comprehensive assessment of immune cell infiltration and immune activity across the dataset.

Intracerebral Hemorrhage Model Construction

Male C57BL/6 (C57) mice, weighing between 20 and 23 g, were sourced from the Animal Center of the Chinese Academy of Sciences in Shanghai, China. Anesthesia was induced using isoflurane, and the mice were positioned in a stereotactic frame. The surgical procedure included

preparation of the skin, sterilization, and exposure of the skull under aseptic conditions. A small burr hole was drilled into the right hemisphere, avoiding the meninges, with bregma serving as a reference point at coordinates 2.0 mm lateral and 0.6 mm anterior. A microinjector was then positioned 3.0 mm deep in the basal ganglia, delivering 30 µl of non-heparinized autologous blood at a rate of 2 µl per minute. After maintaining the needle in position for 10 min, it was carefully removed. In the control group, the needle was inserted but no blood was injected. The incision was sterilized and closed using silk sutures.

Immunohistochemistry (IHC)

The immunoreactivity of Gls was evaluated using immunohistochemistry in accordance with standard procedures. The primary antibody used for this purpose was Gls (diluted at 1:200, sourced from Proteintech, catalog number 66265–1-Ig). For detection, the secondary antibody kit GTVisionTM III Detection System/Mo&Rb (including DAB) was applied, obtained from Genetech, Shanghai, China. Following the immunostaining process, tissue sections were counterstained with hematoxylin, which was supplied by KeyGEN BioTECH, Jiangsu, China. All microscopic images of the stained sections were captured using an ECLIPSE Ti2 microscope from Nikon, Japan.

Real-Time Quantitative PCR (qRT–PCR)

Perihematomal brain tissue was collected, and total RNA was isolated using the TRIzol extraction method. Complementary DNA (cDNA) synthesis was performed using the RT Master Mix from MedChemExpress (Shanghai, China) with the qPCR II system. Real-time PCR analysis followed, using the SYBR Green qPCR Master Mix (also from MedChemExpress), to assess gene expression levels. The $2^{-\Delta\Delta CT}$ method was applied to quantify gene expression. Three technical replicates were set for each sample, with β-actin used as the internal reference gene. All amplification curves showed a single peak, and the melting curves exhibited characteristics of a single product. The primer sequences used in this analysis are listed in Table 1.

Statistical Analysis

Statistical analysis was performed using GraphPad Prism 9 (GraphPad Software, CA, USA). To compare the levels of immune cell expression and hub gene expression between the ICH (intracerebral hemorrhage) and control groups, an unpaired t-test was used. P-value < 0.05 was considered statistically significant, indicating a meaningful difference between the two groups.

Table 1 Primers for qRT-PCR

Genes	Primers (5′−3′)
Mtf1-forward	GACCTAACCCCGCATGACAAG
Mtf1-reverse	CCACACTGTCCATCGTCTTCA
Slc31a1-forward	TATGAACCACACGGACGACAA
Slc31a1-reverse	GCCATTTCTCCAGGTGTATTGA
Dld-forward	ACACTAGGTGGAACATGCTTG
Dld-reverse	CAAATCCATTGACGTGAACAACC
Dlat-forward	TAGTCCTCTTGCGAAGAAGTTGG
Dlat-reverse	TCACTCGACGAATGTTGCTGA
Pdhb-forward	GTGGAAGAAATACGGTGACAAGA
Pdhb-reverse	ACCTGGTCAATAGCTTGCATAGA
Gls-forward	TTTCCAGAAGGCACAGACA
Gls-reverse	GGGCAGAAACCACCATTAG
Pdha1-forward	TCATTCGTGGTTTCTGTCA
Pdha1-reverse	CCTCCTCTTCGTCCTGTTAG
β-actin-forward	AACAGTCCGCCTAGAAGCAC
β-actin-reverse	CGTTGACATCCGTAAAGACC

Results

GEO Data Merging and DEGs Identification

The integrated dataset, comprising six ICH samples and six control samples from GSE228222 and GSE200575, was created after removing batch effects from the GEO platform data (Fig. 1A and B). Using the"limma"package, we identified a total of 8,254 differentially expressed genes (DEGs), including 2,658 up-regulated and 5,596 down-regulated genes. The corresponding volcano plot and heat map of these DEGs are presented in Fig. 1C and D.

Functional Enrichment Analysis of DEGs

We conducted GO and KEGG pathway enrichment analyses in R to investigate the potential roles of DEGs. GO enrichment analysis for BP highlighted the involvement of autophagy, cellular component disassembly, processes utilizing autophagic mechanisms, and exocytosis. For CC, the DEGs were enriched in postsynaptic specialization, asymmetric synapse, dense postsynaptic density, and the cell leading edge. MF analysis revealed enrichment in phospholipid binding, GTPase regulator activity, nucleoside-triphosphatase regulator activity, and actin binding (Fig. 2A). KEGG pathway analysis demonstrated that the DEGs were significantly enriched in several key pathways, including the MAPK signaling pathway, chemokine signaling pathway, sphingolipid signaling pathway, neurotrophic pathway, apoptosis, and the P53 signaling pathway (Fig. 2B).

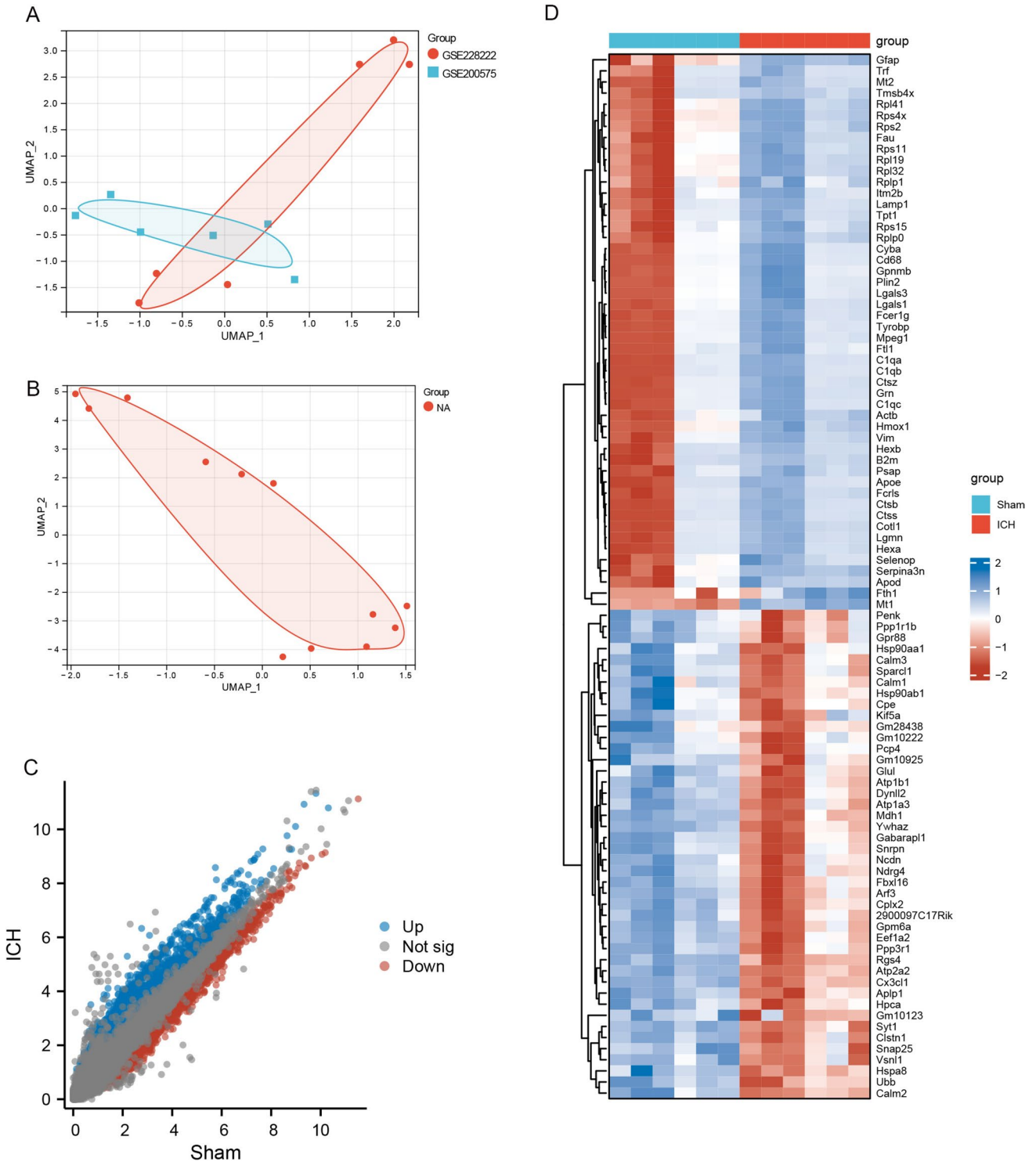

Fig. 1 Differential analysis of the GSE228222 and GSE200575 datasets. **A** Before batch effect removal, the data distribution was discrete. **B** After batch effect removal, the data distribution became concentrated. **C** The differential analysis after batch effect removal identified 8,254 differentially expressed genes. **D** Heatmaps were generated for the top 50 upregulated and downregulated differentially expressed genes

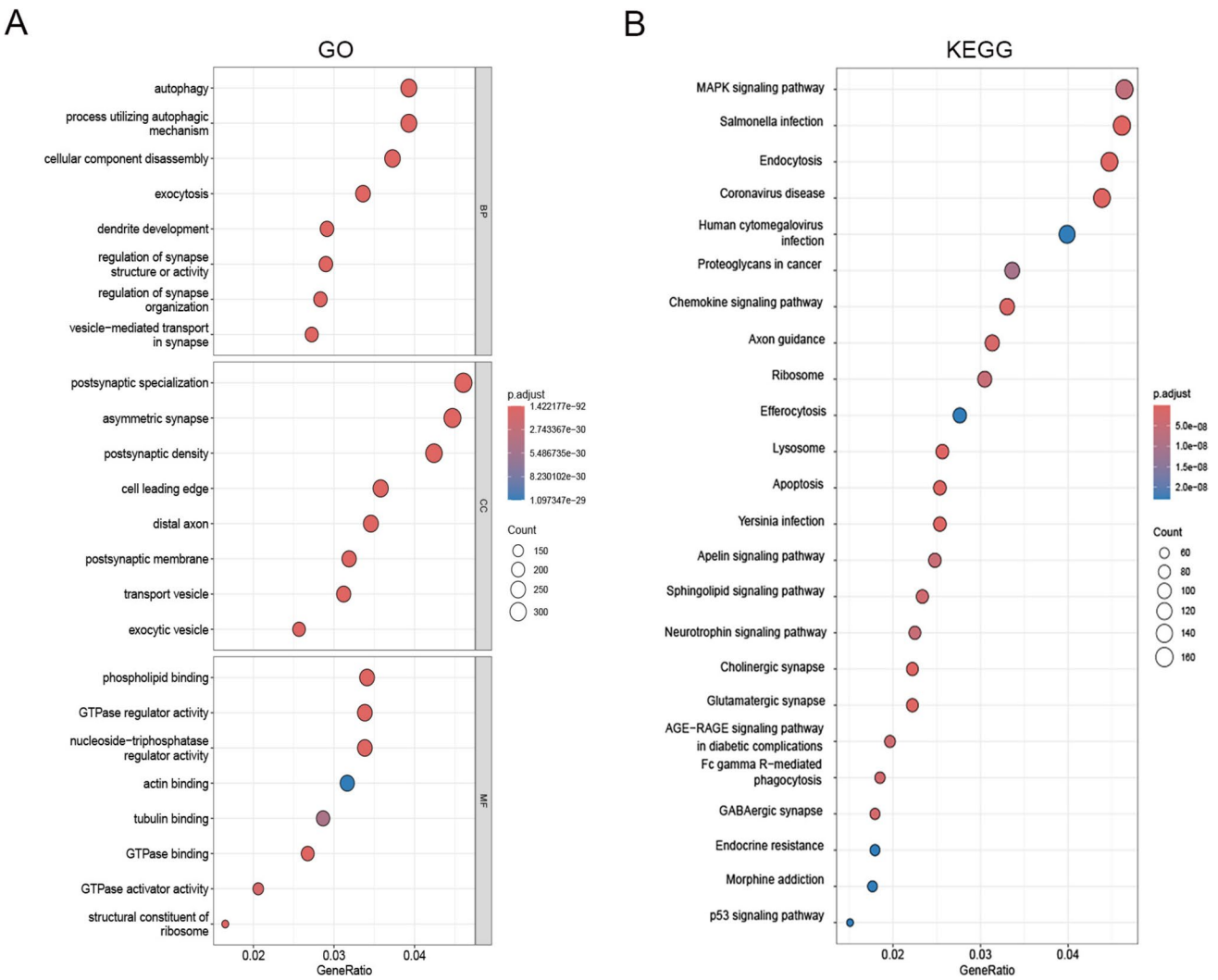

Fig. 2 Enrichment analysis of DEGs. **A** Gene Ontology (GO) enrichment analysis and **B** Kyoto Encyclopedia of Genes and Genomes (KEGG) pathway analysis of ICH DEGs in datasets

Evaluation of Immune Cell Infiltration

Building on previous findings of secondary inflammation and immune responses following ICH (Han et al. 2023; Wilkinson et al. 2018; Zille et al. 2017), we conducted an immune cell infiltration analysis using the CIBERSORT algorithm to further investigate immune regulation after ICH. Box plot analysis revealed that ICH samples had increased proportions of M0 macrophages, M1 macrophages, and naive CD8 T cells. Conversely, the proportions of resting NK cells, follicular CD4 T cells, and naive CD4 T cells were reduced (Fig. 3A).

Figures 3B and 3 C illustrate the expression levels and corresponding proportions of immune cells across the grouped samples. Additionally, correlation analysis among 11 immune cell types indicated no significant correlation between TH17 and TH1 cells. However, strong correlations were observed between follicular CD4 T cells and M0 macrophages ($r = -0.97$), follicular CD4 T cells and M1 macrophages ($r = -0.97$), and M0 macrophages with M1 macrophages ($r = 0.97$) (Fig. 3D).

Identification and Enrichment Analysis of CuDEGs

We plotted the 8,254 differentially DEGs and 12 CRGs on a Venn diagram and identified seven overlapping genes: Pdha1, Gls, Dld, Pdhb, Dlat, Mtf1, and Slc31a1 (Fig. 4A). Functional enrichment analysis of these seven CuDEGs, performed on the WebGestalt platform, revealed associations with the citrate cycle, pyruvate metabolism, and glycolysis/gluconeogenesis pathways (Fig. 4B). Similarly, analysis using GeneMANIA indicated that the CuDEGs were linked to the acyl-CoA metabolic process, the oxidoreductase

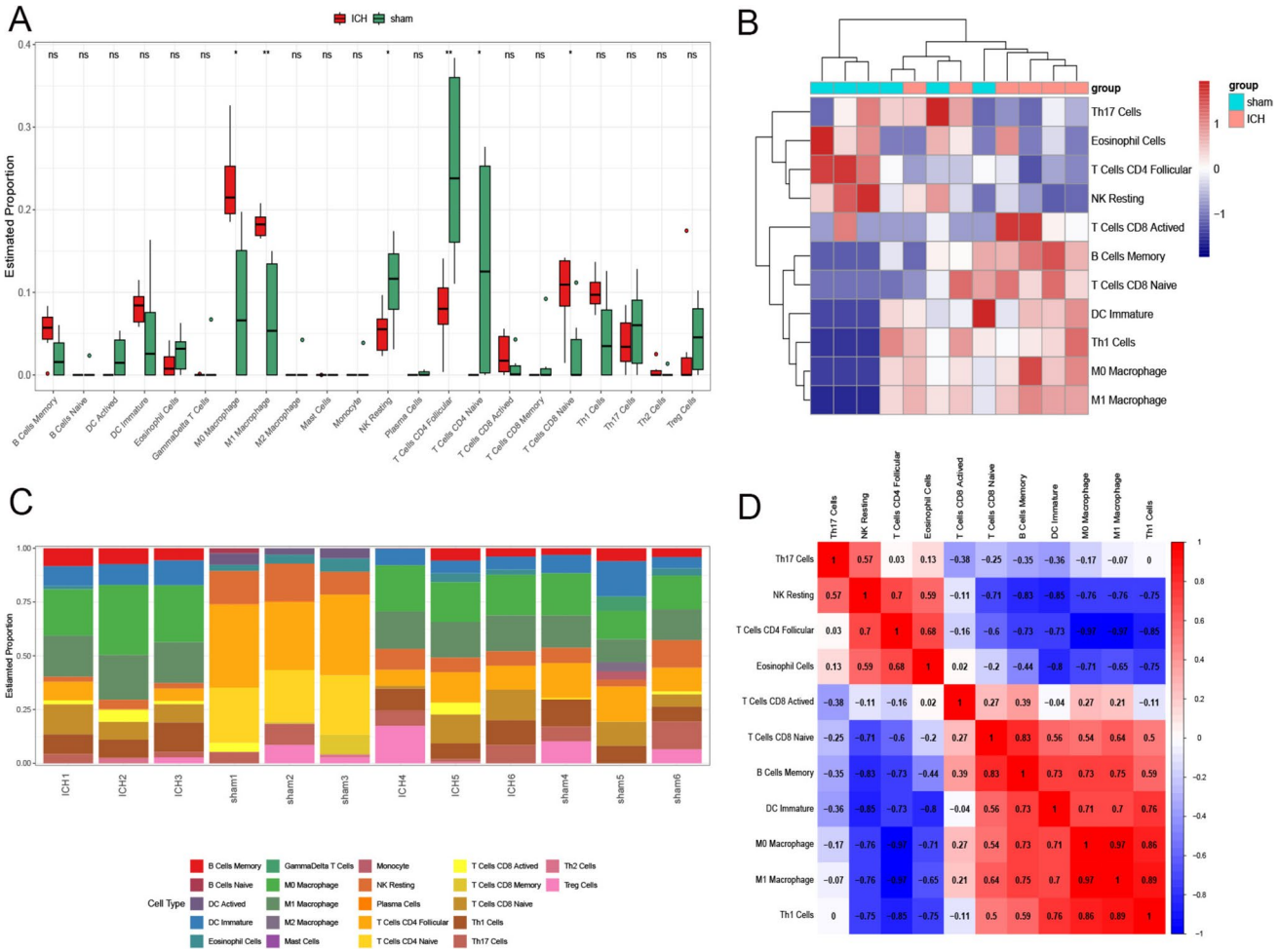

Fig. 3 Immune infiltration analysis of DEGs. **A** Box plots suggested changes in immune cells in ICH and control samples. **B** Heatmap reflected changes in immune cell expression in ICH and control samples. **C** Immune cell components of grouped samples were shown. **D** We showed the interrelationships between immune cells in the form of a heat map

complex, and the glutamine family amino acid biosynthetic process (Fig. 4C).

We also conducted GO and KEGG enrichment analyses on 27 genes identified via GeneMANIA. For BP, these genes were involved in the acyl-CoA metabolic process, thioester metabolic process, acetyl-CoA metabolic process, and acetyl-CoA biosynthetic process from pyruvate. In terms of CC, they were linked to the oxidoreductase complex, dihydrolipoyl dehydrogenase complex, tricarboxylic acid cycle enzyme complex, and mitochondrial protein-containing complex. MF analysis indicated involvement in oxidoreductase activity, specifically acting on the aldehyde or oxo group of donors, and S-acyltransferase activity (Fig. 4D and E). Additionally, KEGG pathway analysis reflected that these 27 genes were involved in carbon metabolism, lipoic acid metabolism, and the citrate cycle, among other pathways. Lastly, we assessed the overall expression of CuDEGs in the combined ICH dataset, as shown in Fig. 4F. In addition to slc31a1, other CuDEGs exhibited lower expression in ICH samples compared to control samples, aligning with the results of our analysis.

Correlation Between CRGs Expression and Immune Infiltration Levels

To further clarify the connection between individual CuDEGs and immune infiltration following ICH, we conducted ssGSEA for each sample. This approach enabled us to assess the enrichment of immune-related gene sets in relation to specific CuDEGs, providing insights into how these genes influence immune cell infiltration in the context of ICH. Box plot analysis revealed that the majority of immune cells exhibited increased infiltration in ICH samples, with the exception of CD4 T cells, which were reduced in ICH samples (Fig. 5A). Correlation analysis showed that CD4 T cells were positively correlated with the CuDEGs

Gls, Dld, Dlat, Pdhb, Pdha1, and Mtf1, but negatively correlated with Slc31a1. Interestingly, Slc31a1 was uniquely negatively correlated with CD4 T cells, while the other six genes showed positive correlations (Fig. 5B). Figures 5C–F further depict the relationships between CuDEGs and various immune-related functions, including immunostimulatory and immunoinhibitory roles, as well as associations with chemokines and chemokine receptors. Lastly, to clarify the functional roles of these seven CuDEGs, we performed ssGSEA-KEGG pathway enrichment analysis. The results demonstrated that these genes were significantly enriched in key signaling pathways, including the TGF-β signaling pathway, MAPK signaling pathway, and B-cell receptor signaling pathway (Fig. 6).

qRT-PCR Analysis of CuDEGs Expression and Immunohistochemistry

We utilized qRT-PCR to validate the expression levels of the seven identified CuDEGs in ICH samples, including Pdha1, Gls, Dld, Pdhb, Dlat, Mtf1, and Slc31a1 (Fig. 7A–G). The qRT-PCR results indicated that the expression of all seven CuDEGs was significantly lower in the ICH samples compared to the control group, which aligns with the findings from our initial analysis. However, in human samples, only GLS showed a significant reduction in expression in ICH samples compared to controls (S1 Fig).

Finally, immunohistochemistry was employed to assess the expression of Gls in both ICH and control tissues. The results confirmed the qPCR findings, with statistical analysis showing significantly lower expression of Gls in ICH tissues compared to the control group (Fig. 7H and I).

Discussion

In this study, we identified a set of DEGs in a mouse ICH dataset by mining the Gene GEO database. Through our analysis, we confirmed the role of inflammation in secondary injury following ICH by examining immune cell infiltration. We then intersected these DEGs with CRGs to identify seven key CuDEGs: Gls, Dld, Pdha1, Dlat, Pdhb, Mtf1, and Slc31a1. PPI networks were constructed for these genes, and immune correlation analyses were performed. To obtain more insights into the potential mechanisms of these seven genes, we conducted GSEA and pathway enrichment analyses across multiple pathways. We observed frequent enrichment in the MAPK signaling pathway and TGF-beta signaling pathway. Additionally, enrichment in the B-cell receptor signaling pathway further supported the pivotal role of immuno-inflammation in the activation of cuproptosis following ICH. We validated our findings using the human ICH dataset GSE24265 and found that only the expression of Gls followed the same trend as in the mouse model. Additionally, the qPCR results for Gls were in alignment with our computational analysis, further supporting its involvement in ICH-related cuproptosis and immune regulation.

The Gls gene, involved in cuproptosis, emerged as a differentially expressed gene in both our differential analyses, suggesting that it may serve as a critical target for modulating cuproptosis to intervene in intracerebral hemorrhage (ICH). Notably, no prior studies have examined the role of Gls in ICH. Gls is the first rate-limiting enzyme in glutamine metabolism, catalyzing the deamination of glutamine to produce glutamate and ammonia (Yu et al. 2019). Glutamate is a key excitatory neurotransmitter in the central nervous system (Zhou et al. 2014), but excessive glutamate can lead to excitotoxicity, resulting in neuronal injury and death (Budgett et al. 2022; Ribeiro et al. 2017). Previous studies have shown that the TGF-β signaling pathway increases Gls mRNA expression, and the transcription factor STAT1 binds to the Gls1 promoter to upregulate Gls1 expression (Zhao et al. 2012), consistent with our GSEA analysis (Andratsch et al. 2007). Moreover, Gls is implicated in the cuproptosis process, tumor mutation, and immune evasion in glioma cells, where patients in the high-risk Gls group exhibited significantly lower survival rates than those in the low-risk group (Ouyang et al. 2022). In addition, Gls has been shown to promote neuroinflammation by activating microglia and facilitating the secretion of pro-inflammatory extracellular vesicles (Ding et al. 2021). Inhibition of Gls has been linked to reduced glycolytic activity by decreasing Hif1 protein in Th17 cells, providing therapeutic benefits in systemic lupus erythematosus (SLE) (Kono et al. 2019). Furthermore, the conversion of glutamine to glutamate by GLS plays a crucial role in T cell function, influencing both the promotion and inhibition of Th17 responses, making Gls a potential target for controlling inflammatory diseases (Johnson et al. 2018).

In our study, we observed a decrease in Gls expression following ICH, which could result in reduced glutamate production. Regarding the observed Gls downregulation, while we propose this reflects an endogenous neuroprotective response to limit glutamate toxicity, alternative interpretations merit consideration. First, compensatory upregulation of alternative ammonia-metabolizing enzymes (e.g., glutamate dehydrogenase) in astrocytes might mitigate metabolic stress (Wilhelm et al. 2012). Second, persistent Gls suppression could impair glutamine-to-GABA conversion in inhibitory neurons, paradoxically exacerbating excitability (Huang et al. 2021). These findings suggest that targeting Gls could offer a novel therapeutic strategy for improving ICH prognosis by modulating glutamate levels and immune responses. Pharmacological inhibition (e.g., repurposing brain-permeable glutaminase inhibitors), cell-specific epigenetic silencing via CRISPR systems delivered by nanoparticles, and copper chelation synergy may be effective therapeutic approaches

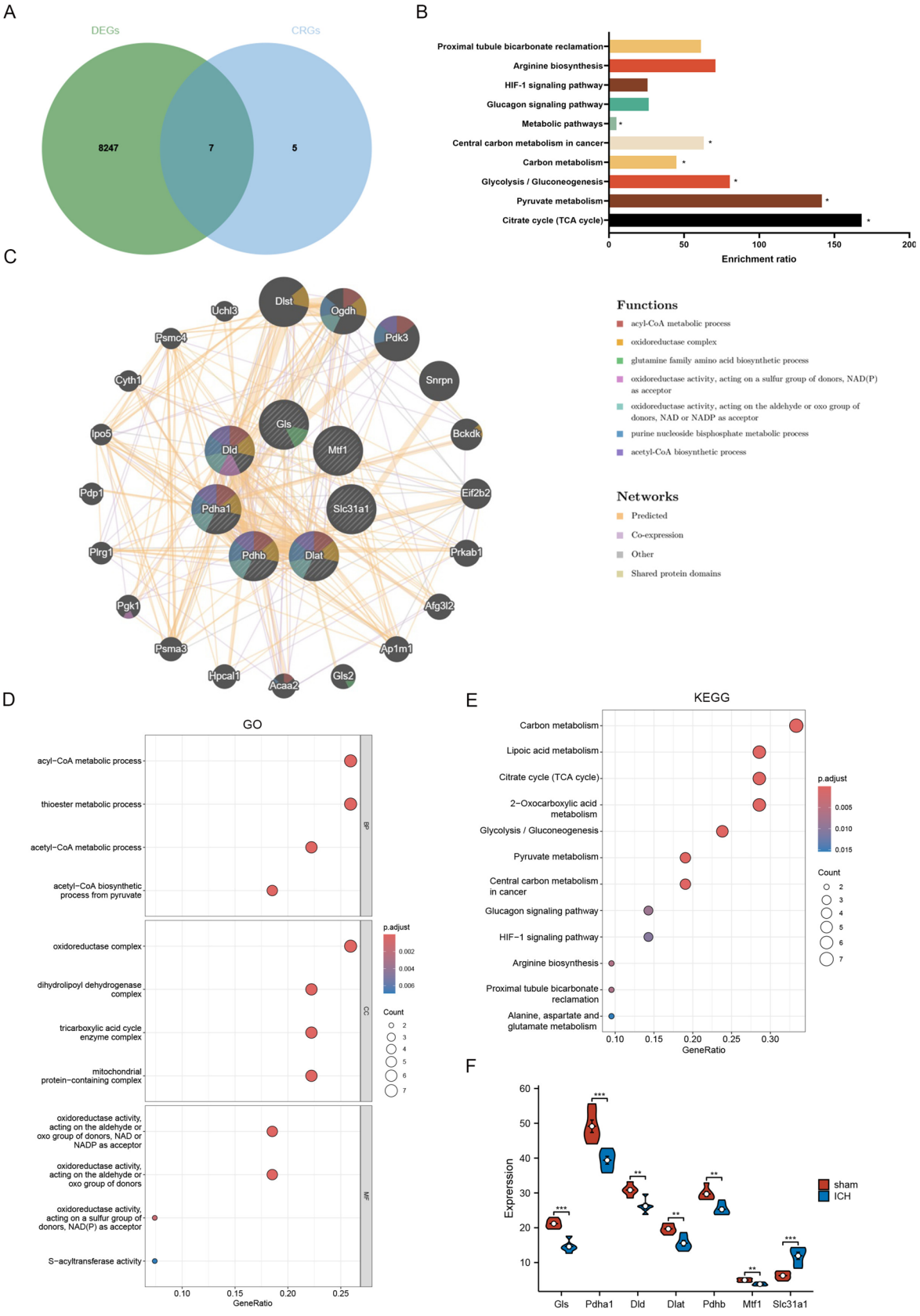
A
DEGs
CRGs
8247
7
5
B
Proximal tubule bicarbonate reclamation
Arginine biosynthesis
HIF-1 signaling pathway
Glucagon signaling pathway
Metabolic pathways
Central carbon metabolism in cancer
Carbon metabolism
Glycolysis / Gluconeogenesis
Pyruvate metabolism
Citrate cycle (TCA cycle)
0
50
100
150
200
Enrichment ratio
C
Dlst
Ogdh
Uchl3
Psmc4
Pdk3
Cyth1
Snrpn
Gls
Ipo5
Dld
Mtf1
Bckdk
Pdp1
Pdha1
Slc31a1
Eif2b2
Plrg1
Pdhb
Dlat
Prkab1
Pgk1
Afg3l2
Psma3
Ap1m1
Hpcal1
Acaa2
Gls2
Functions
acyl-CoA metabolic process
oxidoreductase complex
glutamine family amino acid biosynthetic process
oxidoreductase activity, acting on a sulfur group of donors, NAD(P) as acceptor
oxidoreductase activity, acting on the aldehyde or oxo group of donors, NAD or NADP as acceptor
purine nucleoside bisphosphate metabolic process
acetyl-CoA biosynthetic process
Networks
Predicted
Co-expression
Other
Shared protein domains
D
GO
acyl−CoA metabolic process
thioester metabolic process
acetyl−CoA metabolic process
acetyl−CoA biosynthetic process from pyruvate
oxidoreductase complex
dihydrolipoyl dehydrogenase complex
tricarboxylic acid cycle enzyme complex
mitochondrial protein−containing complex
oxidoreductase activity, acting on the aldehyde or oxo group of donors, NAD or NADP as acceptor
oxidoreductase activity, acting on the aldehyde or oxo group of donors
oxidoreductase activity, acting on a sulfur group of donors, NAD(P) as acceptor
S−acyltransferase activity
BP
CC
MF
p.adjust
0.002
0.004
0.006
Count
2
3
4
5
6
7
0.10
0.15
0.20
0.25
GeneRatio
E
KEGG
Carbon metabolism
Lipoic acid metabolism
Citrate cycle (TCA cycle)
2−Oxocarboxylic acid metabolism
Glycolysis / Gluconeogenesis
Pyruvate metabolism
Central carbon metabolism in cancer
Glucagon signaling pathway
HIF−1 signaling pathway
Arginine biosynthesis
Proximal tubule bicarbonate reclamation
Alanine, aspartate and glutamate metabolism
p.adjust
0.005
0.010
0.015
Count
2
3
4
5
6
7
0.10
0.15
0.20
0.25
0.30
GeneRatio
F
Expression
60
50
40
30
20
10
Gls
Pdha1
Dld
Dlat
Pdhb
Mtf1
Slc31a1
sham
ICH

◂**Fig. 4** Identification of hub genes in ICH and cuproptosis. **A** Differential genes of ICH and CRGstook intersections. **B** Enrichment analysis of 7 CuDRGs was on the WebGestalt. **C** Protein–protein interaction network analysis in GeneMANIA. **D**, **E** GO and KEGG enrichment analysis were done on the basis of all genes given in Figure C. **F** Ladder diagram of differences in expression of CuDRGs in ICH and control samples

for targeting Gls. However, clinical translation will require temporal precision, biomarker-guided dosing, and a balance between neuroprotection and metabolic risks.

Following ICH, secondary injury is primarily driven by inflammation, which exacerbates neuronal death through inflammatory neuronal necrosis mediated by various pro-inflammatory mediators (Zille et al. 2017). Several inflammatory mediators, including Ccl5 (C–C motif chemokine 5), have been previously reported in the literature (Lin et al. 2023). In our analysis, we found that two chemokines associated with Gls are Ccl26 (C–C motif chemokine 26) and Ccl28 (C–C motif chemokine 28). Ccl26 is a chemotactic cytokine from the CC family, also known as eosinophil-specific chemokine 26, and is involved in regulating eosinophil accumulation, particularly in allergic disease models such as lung inflammation (Lloyd et al. 2003). In earlier studies, IL-13 receptor alpha 2 was shown to elevate Ccl26 expression in atopic dermatitis, which exacerbated the inflammatory response (Xiao et al. 2021). However, the role of Ccl26 in ICH has not yet been explored. Since we observed a positive correlation between Gls and Ccl26, we hypothesize that after ICH, the decreased expression of Gls could lead to a corresponding decrease in Ccl26 expression, potentially reducing the inflammatory response. However, the specific mechanisms underlying this relationship remain to be investigated. Ccl28, also a CC family chemokine, is known as mucosa-associated epithelial chemokine and serves as a ligand for Ccr10. It is secreted by epithelial cells in organs such as the intestines, lungs, mammary glands, and salivary glands (Pan et al. 2000; Wang et al. 2000). Ccl28 is constitutively expressed in colonic epithelial cells, and its expression is regulated by pro-inflammatory cytokines and bacterial products, suggesting a role in attracting Ccr10 + cells to sites of colonic inflammation (Hieshima et al. 2003). In rheumatoid arthritis, Ccl28 has been shown to mediate the inflammatory response by promoting angiogenesis and endothelial cell migration through activation of the ERK signaling pathway (Pan et al. 2015). In our study, the expression of Ccl28 was positively correlated with Gls. We hypothesize that the decrease in Gls expression following ICH could also result in a reduction in Ccl28 expression, thereby contributing to a decrease in the inflammatory response. However, like Ccl26, the exact mechanisms by which Ccl28 affects inflammation after ICH require further investigation.In summary, both Ccl26 and Ccl28 may play significant roles in the inflammatory response following ICH, with their expression potentially regulated by Gls. The reduction in Gls expression after ICH could be a self-protective mechanism that lowers the levels of these chemokines, thereby mitigating inflammation. Further research is needed to explain the mechanisms at work.

Based on our findings from immune infiltration analysis and the correlation of CRGs, we observed increased expression of M0 macrophages, M1 macrophages, and naive CD8 T cells, along with decreased expression of resting NK cells, follicular CD4 T cells, and naive CD4 T cells in the ICH model. Notably, CD4 T cells were positively correlated with the expression of Gls. Our current study aligns with previous research showing that recombinant human Ccl28 exhibits chemotactic activity for resting CD4 T cells in vitro (Wang et al. 2000). Therefore, the reduced expression of Gls in ICH may lead to lower Ccl28 expression, consequently diminishing CD4 T cell activation, which is consistent with our observations. During the acute and subacute phases of ICH, lymphocytes accumulate near the hematoma, along with activated brain cells like microglia and astrocytes. Various lymphocyte subsets, including CD4 T cells, CD8 T cells, B cells, and NK cells, are detectable within one day post-ICH, with their presence peaking around three days (Loftspring et al. 2009; Mracsko et al. 2014; Li et al. 2020). Previous studies have shown that CD4 T cells promote localized inflammation via IL-17, and depletion of CD4 T cells can reduce secondary injury after ICH (Shi et al. 2023). These findings are in line with the results of our analysis, which demonstrated decreased CD4 T cells in ICH samples. Although the role of CRGs in ICH immunomodulation has not been extensively studied, our data suggest that CRGs could be critical in immune cell infiltration following ICH. The correlation between Gls and CD4 T cells, coupled with the decrease in Ccl28 expression, indicates a potential mechanism by which CRGs might regulate immune responses in ICH. Although our data demonstrate significant correlations between cuproptosis-related gene expression (particularly Gls) and immune cell infiltration patterns, these associations should be interpreted cautiously due to inherent limitations in establishing causation. This highlights the need for further investigation into the precise role of CRGs in ICH immune infiltration and inflammatory regulation.

Not with standing these findings, several limitations should be acknowledged. First, while our integrated bioinformatics approach identified conserved CRGs signatures across species, the exclusive reliance on GEO datasets may introduce selection bias, particularly given the limited sample size. Second, the translational relevance of our findings is constrained by the use of postmortem human specimens in GSE24265, where agonal changes may alter gene expression profiles. Furthermore, bulk RNA-seq data cannot resolve cell-type-specific dynamics—a critical gap given emerging evidence that microglia exhibit distinct copper metabolism pathways compared

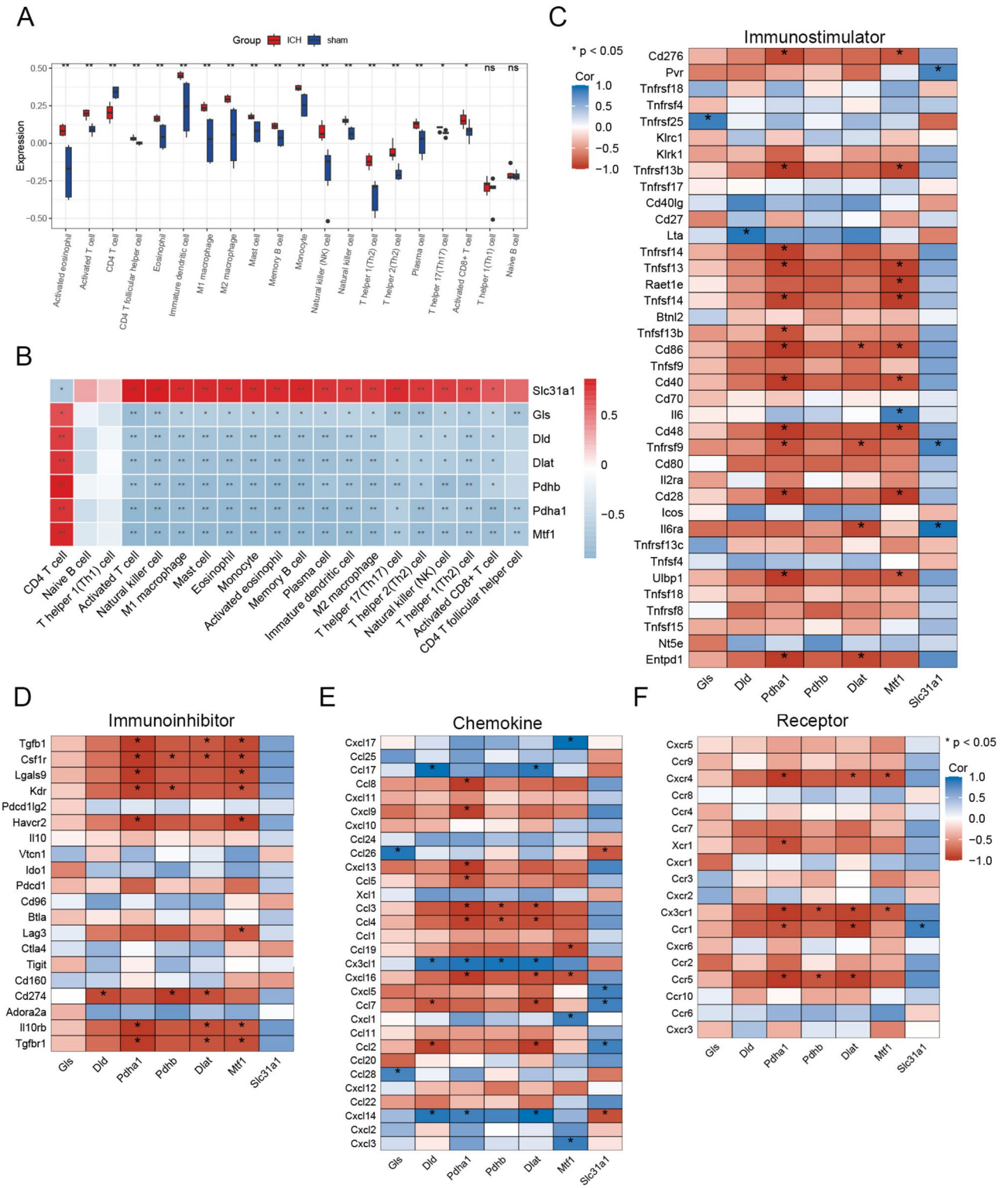

Fig. 5 Single gene immunoinfiltration analysis. **A** Box plots suggested changes in immune cells in ICH and control samples. **B** Correlation between CuDEGs and immune cells. **C**–**F** Correlation between CuDEGs and immunostimulatory, immunoinhibitory, chemokine, chemokine receptor

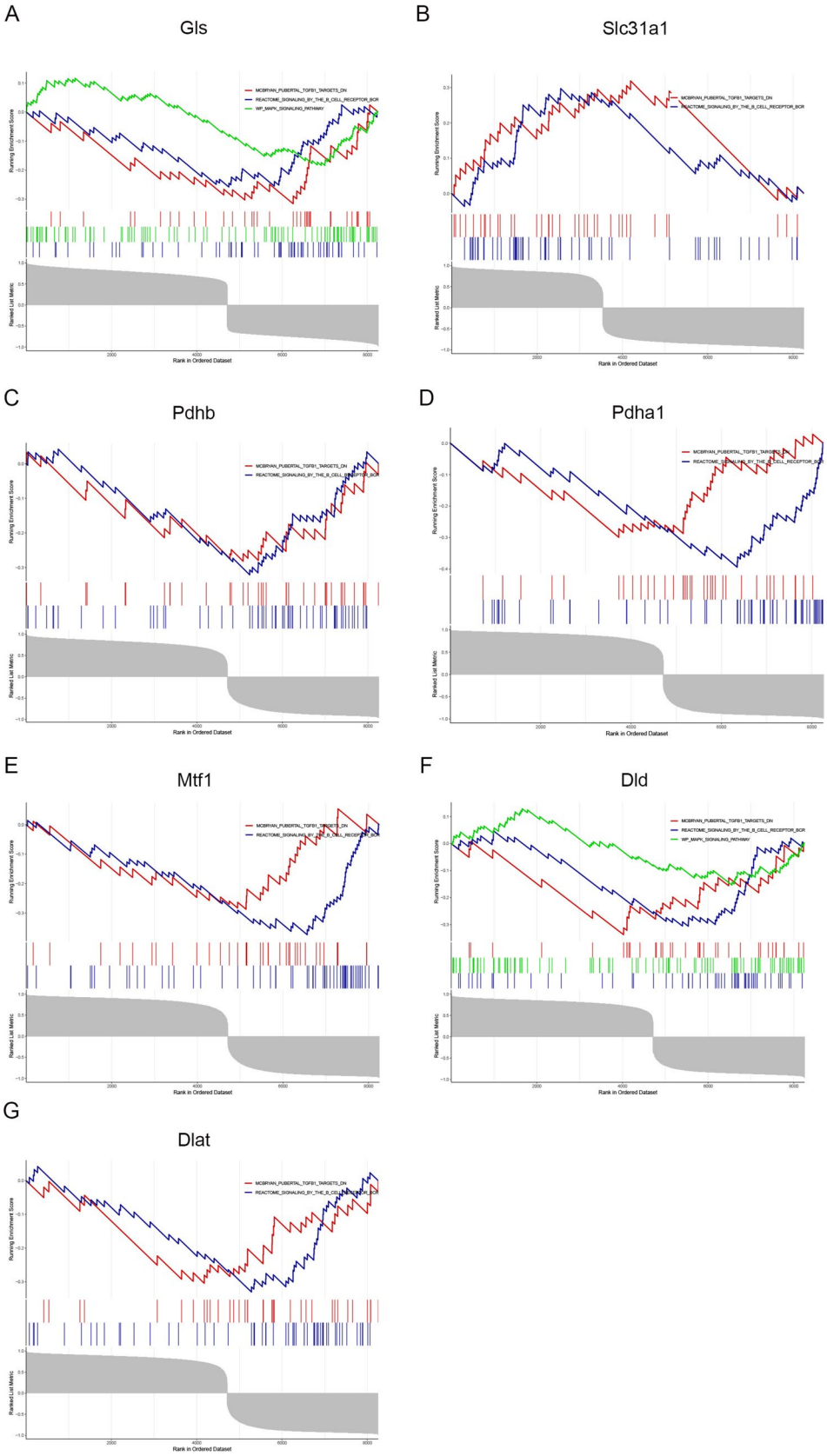

Fig. 6 Single-gene GSEA-KEGG pathway analysis in **A** Gls, **B** Slc31a1, **C** Pdhb, **D** Pdha1, **E** Mtf1, **F** Dld and **G** Dlat

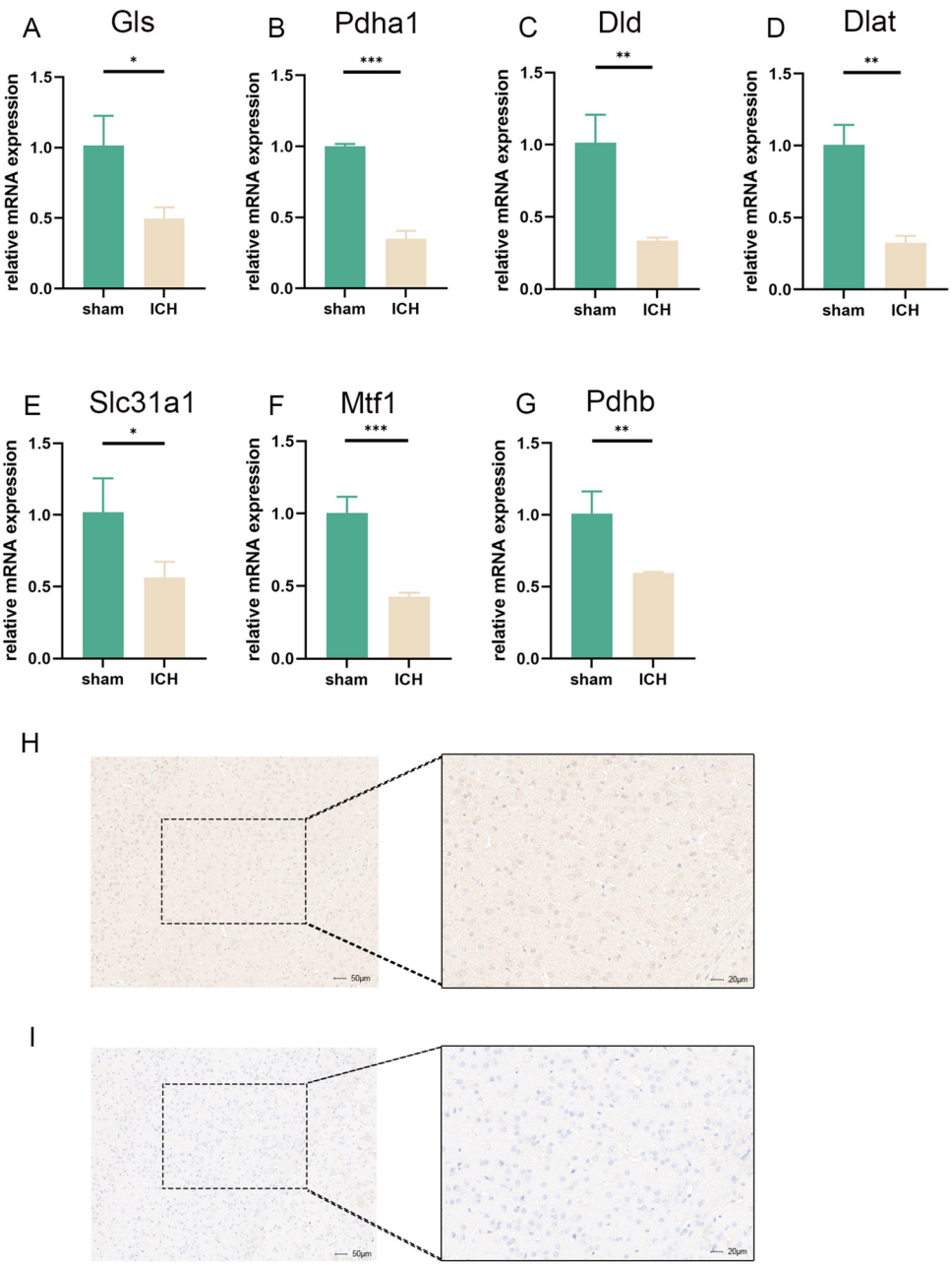

Fig. 7 Expression of CuDEGs in tissues. **A**–**G** Differences in mRNA levels of CuDEGs were verified by qPCR in ICH and control samples. IHC of Gls in control (**H**) and ICH samples (**I**)

to neurons. Finally, while we observed strong correlations between Gls expression and immune infiltration, the temporal sequence of these events remains unclear. Therefore, the validity of our data and conclusions will need further clinical and experimental validation to ensure robustness and applicability.

Conclusion

In summary, Gls was identified as a potential target for cuproptosis intervention in the prognosis of ICH. By reducing its expression in ICH, Gls may help mitigate cuproptosis, thus limiting neuronal damage caused

by excessive glutamate production and decreasing the immune response driven by CD4 T cells. This study provides insights that may contribute to the reduction of cuproptosis progression following ICH and potentially improve the clinical outcomes for patients with ICH. Further investigation and clinical trials are essential to thoroughly evaluate the therapeutic potential of targeting Gls in the treatment of ICH.

Supplementary Information The online version contains supplementary material available at https://doi.org/10.1007/s10571-025-01571-z.

Author contributions Xi Shen conceived the idea and wrote the main manuscript text; Jiandong Zhu designed this research, interpreted data, and revised manuscript; Jinxin lu and Yuhang Gu corrected, edited, and reviewed the manuscript; Weiwei Zhai, Liang Sun, Jiang Wu and Zhengquan Yu approved the final version of the manuscript.

Funding The grant from the Medical and Health Science and Technology Innovation Project of the Suzhou Health Commission, SKY2022002, the grant from the Special Funds for Science and Technology Programs of Jiangsu Provincial Department of Science and Technology, BE2023712.

Data Availability No datasets were generated or analysed during the current study.

Declarations

Conflict of interest The authors declare no competing interests.

Ethical Approval The Medical Ethics Committee of the First Affiliated Hospital of Soochow University approved this study. [Reference number: sdfyy2022-446].

References

Andratsch M, Hu J, Wu X, Hammerman MR (2007) TGF-beta signaling and its effect on glutaminase expression in LLC-PK1-FBPase+ cells. Am J Physiol-Renal Physiol 293(3):F846–F853. https://doi.org/10.1152/ajprenal.00139.2007

Budgett RF, Bradshaw HB, Ward M, Walker SJ, Armstrong DM (2022) Targeting the type 5 metabotropic glutamate receptor: a potential therapeutic strategy for neurodegenerative diseases? Front Pharmacol. https://doi.org/10.3389/fphar.2022.893422

Cordonnier C et al (2018) Intracerebral haemorrhage: Current approaches to acute management. Lancet 392(10154):1257–1268. https://doi.org/10.1016/s0140-6736(18)31878-6

Debrabant B (2017) The null hypothesis of GSEA, and a novel statistical model for competitive gene set analysis. Bioinformatics 33(9):1271–1277. https://doi.org/10.1093/bioinformatics/btw803

Ding L, Ouyang X, Wang H, Liao W (2021) Glutaminase in microglia: a novel regulator of neuroinflammation. Brain Behav Immun 92:139–156. https://doi.org/10.1016/j.bbi.2020.11.038

Han R et al (2023) Improving outcomes in intracerebral hemorrhage through microglia/macrophage-targeted IL-10 delivery with phosphatidylserine liposomes. Biomaterials. https://doi.org/10.1016/j.biomaterials.2023.122277

Han J et al (2024) Roles and mechanisms of copper homeostasis and cuproptosis in osteoarticular diseases. Biomed Pharm. https://doi.org/10.1016/j.biopha.2024.116570

Hänzelmann S, Castelo R, Guinney J (2013) GSVA: gene set variation analysis for microarray and RNA-seq data. BMC Bioinformatics. https://doi.org/10.1186/1471-2105-14-7

Hieshima K, Ohtani H, Shibano M, Izawa D, Nakayama T, Kawasaki Y, Yoshie O (2003) CCL28 has dual roles in mucosal immunity as a chemokine with broad-spectrum antimicrobial activity. J Immunol 170(3):1452–1461. https://doi.org/10.4049/jimmunol.170.3.1452

Huang Q, Lian C, Dong Y, Zeng H, Liu B, Xu N, He Z, Guo H (2021) SNAP25 inhibits glioma progression by regulating synapse plasticity via GLS-mediated glutaminolysis. Front Oncol 11:698835. https://doi.org/10.3389/fonc.2021.698835

Johnson MO, Wolf BJ, Madden MZ, Andrejeva G, Smith AM, Foxwell BMJ, Powell JD (2018) Distinct regulation of Th17 and Th1 cell differentiation by glutaminase-dependent metabolism. Cell 175(7):1780-1795.e19. https://doi.org/10.1016/j.cell.2018.10.001

Kanehisa M, Goto S (2000) KEGG: Kyoto encyclopedia of genes and genomes. Nucleic Acids Res 28(1):27–30. https://doi.org/10.1093/nar/28.1.27

Keep RF, Hua Y, Xi G (2012) Intracerebral haemorrhage: Mechanisms of injury and therapeutic targets. Lancet Neurol 11(8):720–731. https://doi.org/10.1016/s1474-4422(12)70104-7

Kono M, Yoshida N, Maeda K, Suárez-Fueyo A, Kyttaris VC, Kannan Y, Tsokos GC (2019) Glutaminase 1 inhibition reduces glycolysis and ameliorates lupus-like disease in MRL/lpr mice and experimental autoimmune encephalomyelitis. Arthrit Rheumatol 71(11):1869–1878. https://doi.org/10.1002/art.41019

Li Z, Shao X, Liu Q, Wu J, Zhao S, Zheng W (2020) Brain transforms natural killer cells that exacerbate brain edema after intracerebral hemorrhage. J Exp Med. https://doi.org/10.1084/jem.20200213

Li L et al (2021) Risks of recurrent stroke and all serious vascular events after spontaneous intracerebral haemorrhage: Pooled analyses of two population-based studies. Lancet Neurol 20(6):437–447. https://doi.org/10.1016/s1474-4422(21)00075-2

Lim-Hing K, Rincon F (2017) Secondary hematoma expansion and perihemorrhagic edema after intracerebral hemorrhage: from bench work to practical aspects. Front Neurol. https://doi.org/10.3389/fneur.2017.00074

Lin J et al (2023) CCL5/CCR5-mediated peripheral inflammation exacerbates blood-brain barrier disruption after intracerebral hemorrhage in mice. J Trans Med. https://doi.org/10.1186/s12967-023-04044-3

Liu H (2022) Pan-cancer profiles of the cuproptosis gene set. Am J Cancer Res 12(8):4074–4081

Lloyd CM, Rankin SM (2003) Chemokines in allergic airway disease. Curr Opin Pharmacol 3(4):443–448. https://doi.org/10.1016/s1471-4892(03)00069-9

Loftspring MC, Kawano T, Anrather J, Iadecola C (2009) Intracerebral hemorrhage leads to infiltration of several leukocyte populations with concomitant pathophysiological changes. J Cereb Blood

Flow Metab 29(1):137–143. https://doi.org/10.1038/jcbfm.2008.114

Mracsko E, Javidi E, Na S-Y, Kahn A, Liesz A, Veltkamp R (2014) Leukocyte invasion of the brain after experimental intracerebral hemorrhage in mice. Stroke 45(7):2107–2114. https://doi.org/10.1161/strokeaha.114.005801

Ouyang Z, Huang W, Liu H, Chen J, Li L, Xu B (2022) Bioinformatic profiling identifies glutaminase to be a potential novel cuproptosis-related biomarker for glioma. Front Cell Dev Biol. https://doi.org/10.3389/fcell.2022.982439

Pan J, Kunkel EJ, Gosslar U, Lazarus N, Langdon P, Broadwell K, Butcher EC (2000) A novel chemokine ligand for CCR10 and CCR3 expressed by epithelial cells in mucosal tissues. J Immunol 165(6):2943–2949. https://doi.org/10.4049/jimmunol.165.6.2943

Pan F, Ding C, Jones G, Cicuttini F (2015) A longitudinal study of the association between infrapatellar fat pad maximal area and changes in knee symptoms and structure in older adults. Ann Rheum Dis 74(10):1818–1824. https://doi.org/10.1136/annrheumdis-2013-205108

Resource TGO (2019) 20 years and still GOing strong. Nucleic Acids Res 47(D1):D330–D338. https://doi.org/10.1093/nar/gky1055

Ribeiro FM, Vieira LB, Pires RGW, Olmo RP, Ferguson SSG (2017) Metabotropic glutamate receptors and neurodegenerative diseases. Pharmacol Res 115:179–191. https://doi.org/10.1016/j.phrs.2016.11.013

Shi SX, Chen L, Wang L, Cheng C, Lin Q, Wang J (2023) CD4(+) T cells aggravate hemorrhagic brain injury. Sci Adv. https://doi.org/10.1126/sciadv.abq0712

Tang D, Chen X, Kroemer G (2022) Cuproptosis: a copper-triggered modality of mitochondrial cell death. Cell Res 32(5):417–418. https://doi.org/10.1038/s41422-022-00653-7

Tsvetkov P et al (2022) Copper induces cell death by targeting lipoylated TCA cycle proteins. Science 375(6586):1254–1261. https://doi.org/10.1126/science.abf0529

Wang W, Soto H, Oldham ER, Buchanan ME, Homey B, Catron D, Zlotnik A (2000) Identification of a novel chemokine (CCL28), which binds CCR10 (GPR2). J Biol Chem 275(29):22313–22323. https://doi.org/10.1074/jbc.M001461200

Wilhelm F, Hirrlinger J (2012) Multifunctional roles of NAD^+ and NADH in astrocytes. Neurochem Res 37(11):2317–2325. https://doi.org/10.1007/s11064-012-0760-y

Wilkinson DA et al (2018) Injury mechanisms in acute intracerebral hemorrhage. Neuropharmacology 134(Pt B):240–248. https://doi.org/10.1016/j.neuropharm.2017.09.033

Xi G, Keep RF, Hoff JT (2006) Mechanisms of brain injury after intracerebral haemorrhage. Lancet Neurol 5(1):53–63. https://doi.org/10.1016/s1474-4422(05)70283-0

Xiao S, Liu M, Li G, Zhao Y, Lu H (2021) Innate immune regulates cutaneous sensory IL-13 receptor alpha 2 to promote atopic dermatitis. Brain Behav Immun 98:28–39. https://doi.org/10.1016/j.bbi.2021.08.211

Xu M et al (2023) Identification and validation of immune and oxidative stress-related diagnostic markers for diabetic nephropathy by WGCNA and machine learning. Front Immunol. https://doi.org/10.3389/fimmu.2023.1084531

Yu G et al (2012) clusterProfiler: An R package for comparing biological themes among gene clusters. OMICS 16(5):284–287. https://doi.org/10.1089/omi.2011.0118

Yu Y et al (2019) Glutamine metabolism regulates proliferation and lineage allocation in skeletal stem cells. Cell Metab 29(4):966-978.e4. https://doi.org/10.1016/j.cmet.2019.01.016

Zhao L, Huang Y, Cai W, Li H, Wu L, Xu Y, Buch S (2012) Interferon-α regulates glutaminase 1 promoter through STAT1 phosphorylation: Relevance to HIV-1 associated neurocognitive disorders. PLoS ONE 7(3):e32995. https://doi.org/10.1371/journal.pone.0032995

Zhou Y, Danbolt NC (2014) Glutamate as a neurotransmitter in the healthy brain. J Neural Transm (Vienna) 121(8):799–817. https://doi.org/10.1007/s00702-014-1180-8

Zille M et al (2017) Neuronal death after hemorrhagic stroke in vitro and in vivo shares features of ferroptosis and necroptosis. Stroke 48(4):1033–1043. https://doi.org/10.1161/strokeaha.116.015609